JGR Oceans

RESEARCH ARTICLE
10.1029/2020JC016110

Special Section:
The Arctic: An AGU Joint Special Collection

Sea Surface Salinity as a Proxy for Arctic Ocean Freshwater Changes

Séverine Fournier[1], Tong Lee[1], Xiaochun Wang[2], Thomas W. K. Armitage[3], Ou Wang[1], Ichiro Fukumori[1], and Ron Kwok[1]

[1]Jet Propulsion Laboratory, California Institute of Technology, Pasadena, CA, USA, [2]Joint Institute for Regional Earth System Science and Engineering, University of California Los Angeles, CA, Los Angeles, USA, [3]Earth System Science Interdisciplinary Center, University of Maryland, College Park, MD, USA

Key Points:
- Sea surface salinity (SSS) is found to be a good proxy for characterizing fresher changes in much of the Arctic Ocean
- Satellite altimetry-gravimetry measurements can help evaluate satellite SSS, alleviating the paucity of in situ salinity data for validation
- The findings will benefit ongoing cal/val of satellite SSS in the Arctic and ongoing field programs in the Arctic

Correspondence to:
S. Fournier,
severine.fournier@jpl.nasa.gov

Citation:
Fournier, S., Lee, T., Wang, X., Armitage, T. W. K., Wang, O., Fukumori, I., & Kwok, R. (2020). Sea surface salinity as a proxy for arctic ocean freshwater changes. *Journal of Geophysical Research: Oceans*, *125*, e2020JC016110. https://doi.org/10.1029/2020JC016110

Received 26 JAN 2020
Accepted 12 MAY 2020
Accepted article online 19 MAY 2020

Abstract The changing Arctic freshwater content and distribution have a significant implications for ocean circulation, climate, and water and biogeochemical cycles. The paucity of in situ salinity measurements in the Arctic Ocean has limited our ability to study Arctic-Ocean freshwater variability. Although satellite-derived sea surface height (SSH) and ocean bottom pressure (OBP) have been used together to infer depth-integrated freshwater content changes, these measurements are limited in sampling and resolution. Motivated by the recent development of sea surface salinity (SSS) remote sensing, we explore the use of SSS as a proxy for Arctic freshwater changes. As a first step, here we conduct a proof-of-concept study by analyzing the output of an ocean-ice state estimation product. We find that SSS variations are coherent with those of SSH-minus-OBP across the Arctic basin (with $R \sim -0.8$) except for those in the center of the Beaufort Gyre and the region affected by the subpolar North Atlantic inflow. On Arctic shelves, the linear regression coefficient between SSS and SSH-minus-OBP is −0.3 pss/cm or larger in magnitude. The results suggest that SSS is a good proxy for Arctic freshwater changes, and satellite SSH-minus-OBP can be used to evaluate satellite SSS quality.

1. Introduction

The variability of salinity, or alternatively freshwater content (FWC), in the upper few hundred meters of the Arctic Ocean is important for a broad spectrum of processes, including ocean advection, mixing, water mass formation, heat and freshwater budgets, sea ice formation, and ice cover persistence (Bulgakov, 1962; Carmack, Polyakov, et al., 2015; Chen & Tung, 2014; Talley, 2002; Vaughan et al., 2013). The FWC of the upper Arctic Ocean is primarily maintained by river discharge (~40%), precipitation minus evapotranspiration (~25%), and inflow of relatively fresh Pacific water through the Bering Strait (~30%) (Serreze et al., 2006). These fluxes maintain the halocline stratification, insulating Arctic sea ice from the warmer Atlantic-sourced water at depth (e.g., Aagaard et al., 1981). In Arctic waters, salinity dominates seasonal to interannual sea level variability and hence the large-scale geostrophic circulation of the Arctic Ocean (Armitage et al., 2016, 2017; Giles et al., 2012; McPhee et al., 2009; Morison et al., 2012). Freshwater export from the Arctic has implications for the North Atlantic and global oceanic circulation as well as ocean heat content and biogeochemical cycles (Beszczynska-Möller et al., 2011; Chen & Tung, 2014; Li et al., 2009; Pivovarov et al., 2003; Talley, 2002). Thus, monitoring, understanding, and predicting upper Arctic Ocean salinity and FWC has become an important topic of research in recent decades.

The Arctic Ocean has been undergoing drastic changes: It is losing sea ice (e.g., Kwok & Rothrock, 2009), warming (e.g., Polyakov et al., 2005), and freshening (e.g., McPhee et al., 2009). In particular, the liquid freshwater storage increased during the 2000s in the Beaufort Gyre, due to wind-driven accumulation of fresh surface waters by Ekman pumping (Armitage et al., 2016, 2017; Carmack et al., 2016; Giles et al., 2012; Haine et al., 2015; Manucharyan & Spall, 2016; Meneghello et al., 2018; McPhee et al., 2009; Morison et al., 2012; Proshutinsky et al., 2002, 2009; Rabe et al., 2011, 2014). Also, changes in the freshwater fluxes to and from the Arctic Ocean have been reported (Beszczynska-Möller et al., 2011; Carmack et al., 2016; Haine et al., 2015; Köhl & Serra, 2014; Lique et al., 2016; Polyakov et al., 2017; Rabe et al., 2014; Tsubouchi et al., 2012). The 2015 Arctic Report Card (NOAA, 2015) suggested that, in 2014, the combined discharge of the eight largest Arctic rivers was 10% greater than that in the 1980s average. Peterson et al. (2002) reported a 7% increase in Arctic discharge from the six largest Eurasian rivers between 1936

and 1999. Precipitation also has an impact on the freshwater storage distribution (Bintanja & Andry, 2017). Climate models project a strong increase in Arctic precipitation over the coming century (Bintanja & Selten, 2014). Finally, Beszczynska-Möller et al. (2011) emphasize the importance of monitoring freshwater fluxes through the Arctic Ocean gateways, which can impact both Arctic freshwater storage and have wider-reaching climate impacts.

Arctic FWC, and in particular the storage of freshwater in the Beaufort Gyre, has conventionally been monitored by in situ hydrographic measurements from moorings, Conductivity-Temperature-Depth sensors (CTD), and ice-tethered profilers (ITP; e.g., McPhee et al., 2009; Proshutinsky et al., 2009). However, the limited spatiotemporal sampling and coverage of the in situ measurements pose a significant challenge to our ability to monitor Arctic Ocean FWC. High-inclination satellite altimetry (e.g., from CryoSat-2) and time variable gravimetry data from the Gravity Recovery and Climate Experiment (GRACE) have be used together to estimate Arctic Ocean FWC (Armitage et al., 2016; Giles et al., 2012; Morison et al., 2012). The difference between sea surface height anomalies (SSHA) from altimetry and ocean bottom pressure anomalies (OBPA) from GRACE reflect steric sea level integrated over the water column. In the Arctic Ocean, this difference is almost entirely dominated by halosteric (salinity-induced) changes (Köhl, 2014; Pardaens et al., 2011). This method shows good agreement with in situ FWC estimates ($R \sim 0.9$; Armitage et al., 2016; Morison et al., 2012) and has been used to investigate freshwater redistribution within the Arctic basin (Morison et al., 2012), wind-driven accumulation of freshwater in the Beaufort Gyre (Giles et al., 2012), and freshwater exchanges between the deep basin and shelf seas (Armitage et al., 2016). Remote sensing of Arctic Ocean FWC is highly complementary to in situ measurements, in particular because it is possible to extend measurements to the large Arctic shelf seas, which are very poorly sampled (if at all) by hydrographic observations. Satellite-derived SSHA-OBPA measurements provide broad-scale, monthly observations of halosteric changes in the Arctic Ocean; however, they are less accurate than the in situ measurements and, moreover, the effective resolution of the GRACE data is coarse (~300 km), placing a limit on the utility of satellite SSHA-OBPA to study Arctic freshwater changes.

Sea surface salinity (SSS) measurements from spaceborne L band radiometry (~1.4 GHz) are potentially an untapped complimentary data set for studying Arctic FWC with enhanced spatiotemporal sampling. Two SSS missions are currently in operation: the European Space Agency Soil Moisture and Ocean Salinity mission (2009–present, Reul et al., 2012) and the National Aeronautics and Space Administration Soil Moisture Active Passive mission (2015–present, Entekhabi et al., 2014; Tang et al., 2017). These satellites provide SSS estimates in the seasonally ice-free portions of the Arctic Ocean with a spatial resolution of ~40 km and a 2–3 day approximate temporal repeat. NASA salinity-measuring Aquarius mission (2011–2015) had a lower spatial resolution (100–150 km). L band brightness temperatures have a much lower sensitivity to salinity in polar oceans than in lower-latitude oceans (Swift & McIntosh, 1983). As a result, Arctic SSS retrievals from these missions have large uncertainties (Fournier et al., 2019; Garcia-Eidell et al., 2017; Olmedo et al., 2018; Tang et al., 2018; Xie et al., 2019). Root-mean-square differences (RMSD) between in situ and satellite salinity data range between 0.8 and 3 pss in the Arctic basin, decreasing to 0.5–1 pss for sea surface temperature above 5°C (Fournier et al., 2019). In contrast, the uncertainties of satellite SSS in tropical and subtropical oceans are ~0.1–0.2 pss monthly, 1^{o} scales (e.g., Lee, 2016). Nevertheless, salinity signals in the Arctic Ocean can be very large (Carmack, Winsor, et al., 2015), with spatial variation as large as 10 pss and seasonal variation up to 5–10 pss (e.g., Fournier et al., 2019). The large signal-to-noise ratio may render satellite SSS estimates useful in certain regions of the Arctic Ocean, especially in the shelf regions that are strongly influenced by riverine freshwater input.

The paucity of in situ salinity measurements in the ice-free Arctic Ocean (especially on the shelves) presents a challenge for the evaluation of satellite SSS. However, satellite SSHA-OBPA could be useful for assessing the quality of Arctic Ocean SSS if there is a reliable relationship between SSS and SSHA-OBPA variations. Satellite SSS in the Arctic Ocean, if validated through the SSS and SSHA-OBPA relation, could complement the use of satellite altimetry and gravimetry in studying the distribution and circulation of Arctic freshwater because of the better spatiotemporal sampling of satellite SSS.

This motivates the main objectives of this paper: to conduct a proof-of-concept study investigating the relationship between SSS and SSHA-OBPA in the Arctic Ocean and to explore the potential of using SSS as a proxy for regional Arctic FWC. We perform such a proof-of-concept study using an ocean ice state

estimation product. In section 2, we describe the ocean ice state estimation system and assess the estimation product using in situ and satellite measurements. Section 3 presents the relationship between Arctic SSS and SSHA-OBPA anomalies. Our major findings and their broader implications are discussed in section 4. The results have significant implications for the calibration and validation of satellite-derived SSS in the Arctic Ocean as well as for synergy between SSS and SSHA-OBPA to study Arctic Ocean freshwater variability. Addressing these objectives will benefit ongoing Arctic research programs such as the Polar Prediction Program (http://www.polarprediction.net/) and the Stratified Ocean Dynamics in the Arctic (https://www.onr.navy.mil/Science-Technology/Departments/Code-32/All-Programs/Atmosphere-Research-322/Arctic-Global-Prediction/SODA-DRI.aspx).

2. Data and Methods

Our analysis is carried out using Version-4, Release 3 of the Estimating the Circulation and Climate of the Ocean (ECCO; http://www.ecco-group.org) ocean-sea-ice state estimate, referred to as ECCO-v4 hereafter. A brief description of the ECCO system, the ECCO-v4 product, and an assessment of its fidelity in the Arctic Ocean relevant to our investigation is provided in this section.

2.1. ECCO-v4

ECCO-v4 uses the Massachusetts Institute of Technology General Circulation Model (MITgcm; Marshall, Hill, et al., 1997, Marshall, Adcroft, et al., 1997) as the forward model. The native grid for ECCO-v4 is a so-called latitude-longitude-cap (LLC) grid, a global domain that includes the Arctic Ocean, with resolution ranging from 111 km in the tropics to 22 km at high latitudes and 50 vertical levels. The sea ice component consists of separate dynamic and thermodynamic elements that are coupled to the ocean model to solve prognostic equations for ice area, mean snow and ice thickness, and ice velocity (Losch et al., 2010). Further details of the system are described in Forget et al. (2015).

The forward model uses 6-hourly ERA-Interim Reanalysis (Dee et al., 2011; Simmons et al., 2006) as prior surface forcing using the bulk formula of Large and Yeager (2004). The atmospheric state variables are used as control variables to be adjusted (optimized) during the estimation through data assimilation, as described further below. An important novel feature for this investigation is the surface boundary condition for salinity: The ECCO-v4 forward model does not relax SSS to a climatology, a relatively common practice to prevent model drift due to model errors and surface freshwater flux forcing. Moreover, it does not convert surface freshwater flux to SSS tendency using a mean reference salinity as is commonly done in ocean modeling, which precludes salt conservation. Instead, it uses a natural surface freshwater water condition, whereby precipitation adds volume to the top layer, diluting the top-layer salinity (and vice versa for evaporation).

A large suite of satellite and in situ observations are used to constrain the ECCO-v4 solution (Fukumori et al., 2017). In the Arctic, this includes in situ measurements such as Argo temperature and salinity profiles from IFREMER; CTD and XBT temperature and salinity profiles from the World Ocean Database; salinity profiles from the International Council for the Exploration of the Sea (ICES); salinity from ITP (Toole et al., 2011); and mooring observations from the Beaufort Gyre, Fram Strait, Davis Strait, and Bering Strait (Beszczynska-Möller et al., 2012; Curry et al., 2014; Woodgate et al., 2012). Figure 1 shows the spatial distribution of all the in situ data used to constrain ECCO-v4 (that contributed to the time-mean vertical profile of Figure 2) for the Arctic domain. Satellite observations used to constrain ECCO-v4 include along-track sea level anomalies from ERS-1/2, ENVISAT, SARAL/AltiKa, and CryoSat-2, GRACE ocean bottom pressure, AVHRR sea surface temperature, mean dynamic topography from altimetric mean sea surface (Andersen & Knudsen, 2009), and the geoid (Pavlis et al., 2012).

The ECCO-v4 state estimation is based on the adjoint method. A set of "control" variables are adjusted/optimized during the estimation to obtain a least squares fit of the model to the observations over the entire period of the forward model integration. These control variables include the three-dimensional fields of initial conditions, time-varying two-dimensional surface forcing fields, and model mixing parameters (Heimbach et al., 2005). The forward model, forced by the optimized control variables, produces an optimized solution that is dynamically consistent and satisfies the conservation equations. The period

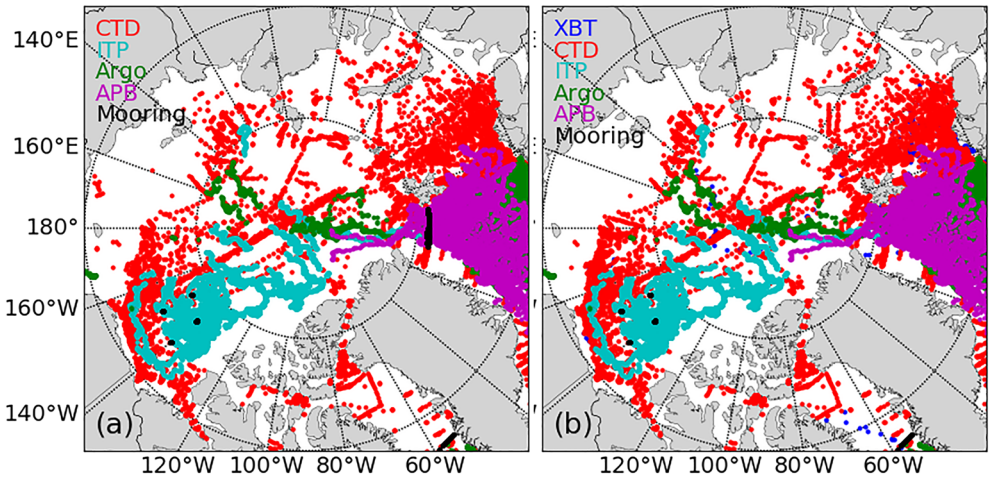

Figure 1. Spatial distribution of all the in situ temperature (a) and salinity (b) data used to constrain ECCO-v4 (that contributed to the time-mean vertical profile of Figure 2) for the Arctic domain.

covered by the ECCO-v4, Release 3 product is 1992–2015. This study focuses on the ice-free Arctic, so we apply the monthly ECCO-v4 ice mask to the SSS, SSH, and OBP outputs from ECCO-v4.

2.2. Assessment of the State Estimates

We assess the ECCO-v4 model by comparing the time mean salinity profile in the upper 500 m of the Arctic Ocean colocated with available in situ data (Figure 2). Salinity variation in the upper 500 m is more relevant to the FWC and halosteric height in the Arctic Ocean (Häkkinen & Proshutinsky, 2004). ECCO-v4 reproduces observed salinity structure in the upper 200 m (the halocline) with a mean difference of −0.02 pss and a RMSD of 0.03 pss. Below 200 m, the differences between the model and the observations are larger with a mean difference of −0.04 pss and a RMSD of 0.04 pss. The larger salinity difference in the deeper ocean might be related to the model's vertical mixing or the representation of the inflow of saline North Atlantic water. There are more in situ measurements in the Nordic Seas per unit area than the rest of the Arctic Ocean (Figure 1). We have also compared the vertical profiles between ECCOv4 and colocated in situ measurements by excluding the data in the Nordic Seas. The results (not shown) are very similar to Figure 2.

Salinity time series for four selected ITPs and the colocated ECCO-v4 data at continuous depths from 0 to 250 m are shown in Figure 3. The ECCO-v4 salinity estimates were linearly interpolated on-the-fly based on the hourly ECCO-v4 outputs and then averaged monthly. The time series include both spatial and temporal variability as the ITPs are advected with the ice pack. ECCO-v4 reproduces the observed salinity variations relatively well. The correlation coefficients between in situ and ECCO-v4 salinity anomalies (referenced to their respective mean profile) range from 0.60 to 0.83 for the four different ITPs. The corresponding mean difference and RMSD between the ITP and ECCO-v4 time series are −0.03, 0.08, −0.03, and 0.02 pss, and 0.32, 0.39, 0.11, and 0.23 pss, respectively (Figure 3). These values are much smaller than the overall dynamic range of the temporal variability of salinity in the Arctic Ocean reported in the literature (e.g., Fournier et al., 2019) as well as illustrated in Figure 3.

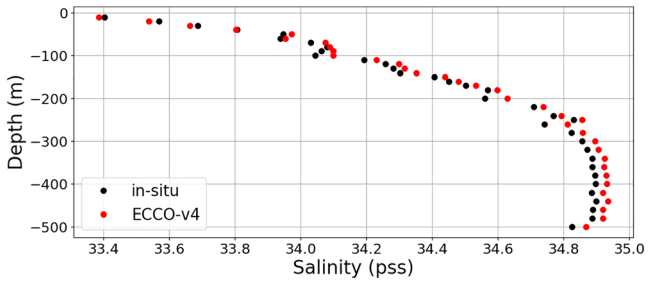

Figure 2. Time-mean salinity profiles from in situ data (black) and colocated ECCO-v4 estimates (red) from 10 to 500 m deep over the period 1992–2015 and for latitudes higher than 65°N.

Because ITPs are under ice, the difference between ECCOv4 and ITP data does not have a direct implication to our focus on the relation between SSS and column-integrated FWC in the ice-free ocean. The comparison with the ITP data was for completeness to provide a sense of fidelity of the freshwater structure of ECCOv4 in the ice-covered ocean. Note that part of the difference between ECCOv4 and ITP data can be related to the difference in spatial scales represented by ECCOv4 (the average value within a cell grid) and ITP (pointwise).

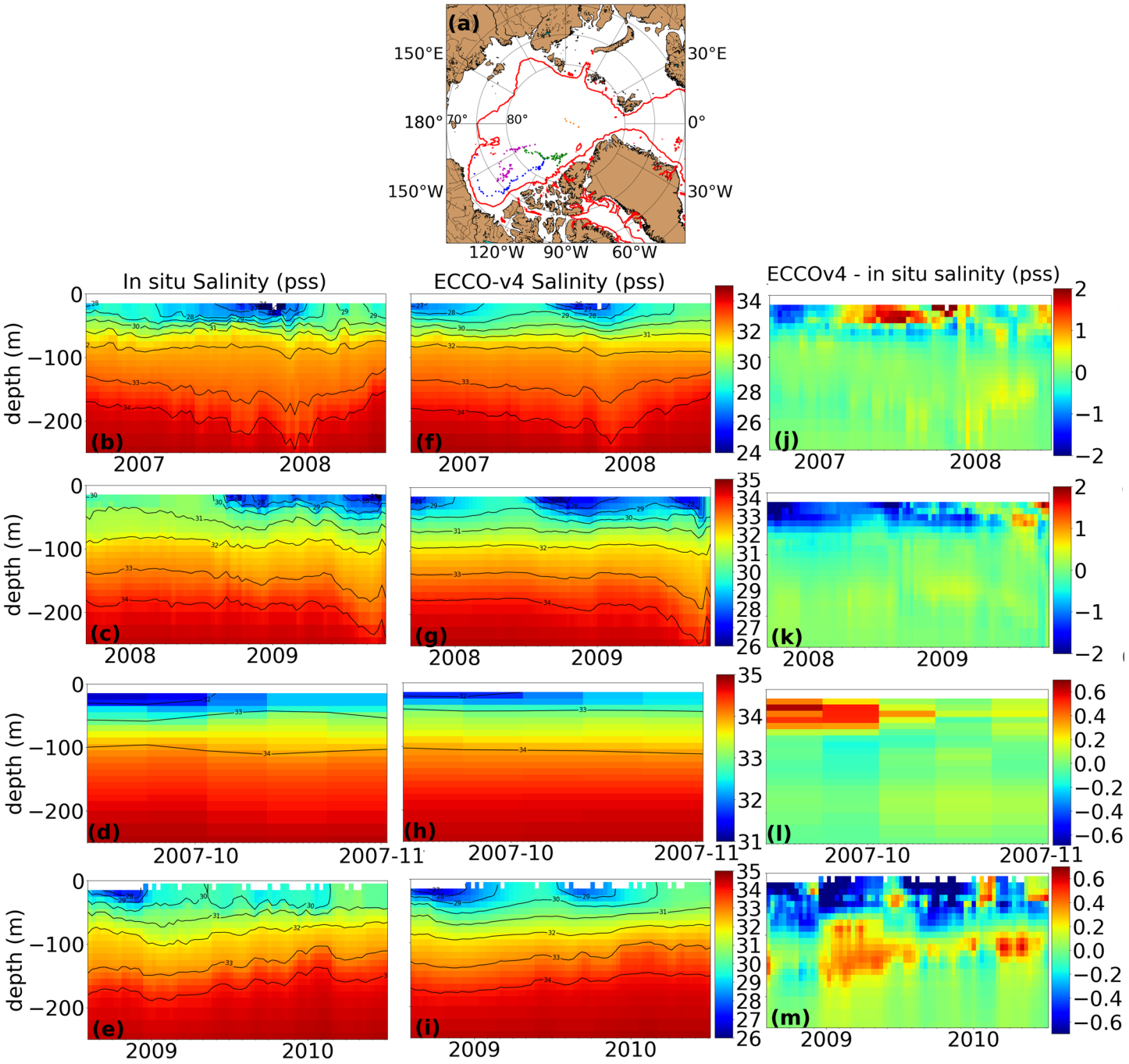

Figure 3. (b–m) Monthly Hovmöller graphs (depth versus time) of in situ (left column), ECCO-v4 (middle column) and ECCO-v4 minus in situ (right column) salinity from selected ITPs of which trajectories are shown in (a) with different colors: Magenta (b, f, j), blue (c, g, k), orange (d, h, l), and green (e, i, m). The red solid line in (a) represents the 500-m isobath contour. The black contours in (b–i) represent salinity contours from 25 to 35 pss every 1 pss.

Figures 4c and 4d show the monthly time series of satellite versus ECCO-v4 SSHA and OBPA averaged over Arctic Ocean regions north of 65°N and deeper than 200 m. The correlation between ECCO-v4 and the satellite data is 0.85 for both SSHA and OBPA. Figures 4a and 4b show the time series of ECCO-v4 versus satellite SSHA and OBPA over the region north of 65°N shallower than 200 m. In this case, the correlation for SSHA and OBPA is 0.84 and 0.78, respectively, slightly (but not substantially) lower than those for the deep regions. This may be due to the limitation of ECCO-v4 in resolving small-scale shelf dynamics as well as the use of river discharge climatology by ECCO-v4 that would reduce interannual salinity variability (and hence

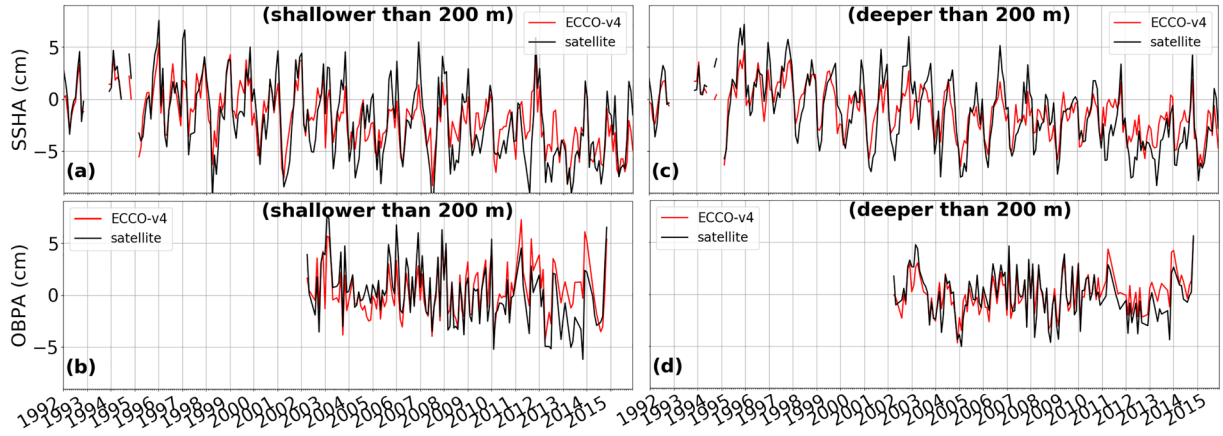

Figure 4. The 1992–2015 monthly time series of ECCO-v4 and satellite SSHA (a–c) and OBPA (b–d) averaged over the region north of 65°N for waters shallower than 200 m (a, b) and deeper than 200 m (c, d). The North Atlantic Ocean and the Barents Sea are excluded from the time series (e.g., excluding longitudes between 40°W and 60°E). The monthly ECCO-v4 ice mask is applied to the model and satellite data.

steric sea level variability) of the shelves associated with river discharge. The slightly lower correlation on the shelves may also be due to greater uncertainty in the satellite data, for instance, land contamination or tidal signals that are not accurately corrected for.

3. Results

In this section, we discuss the temporal correlations between SSS, FWC, SSHA, and SSHA-OBPA based on the ECCO-v4 solution for the period of 1992–2015. In all related figures, only statistically significant correlation values are shown (p value < 0.05) and the ECCO-v4 monthly ice mask is applied to the data. Also, we only consider ice-free pixels that have at least 6 months of data through the period of 1992–2015.

We compute the top-to-bottom FWC following the definition presented in Carmack et al. (2008):

$$FWC = \int_{\mathrm{zlim}}^{0} \left(1 - \frac{S(z)}{Sref}\right) \mathrm{d}z$$

where $S(z)$ is the salinity at depth z, S_{ref} the reference salinity (taken to be 34.8 pss) and z_{lim} the uppermost depth for which S equals S_{ref} or the ocean floor. SSS and FWC are strongly anticorrelated (Figure 5), with

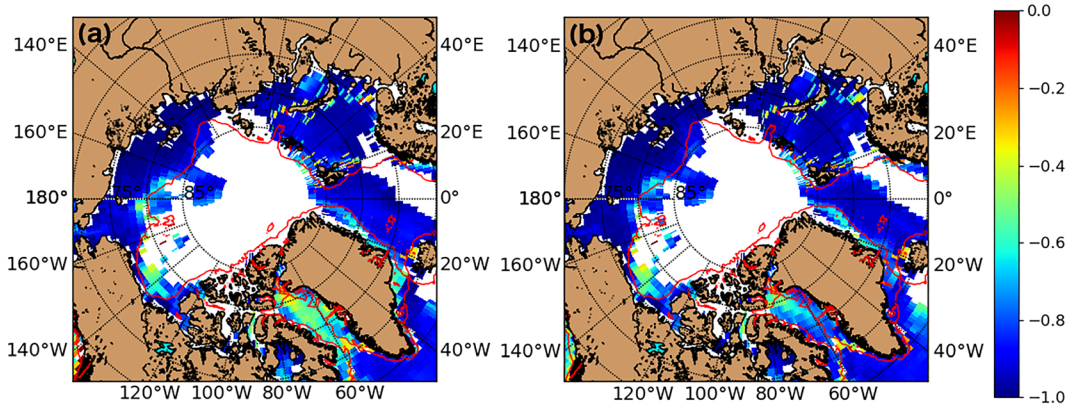

Figure 5. Regional distribution of temporal correlation coefficients during the period 1992–2015 between monthly ECCO-v4 sea surface salinity (SSS) and top-to-bottom freshwater water content with the seasonal cycle included (a) and with the seasonal cycle removed (b). The red solid line represents the 500-m isobath contour. Only significant correlations (p value < 0.05) are shown. The monthly ECCO-v4 ice mask is applied to the model data before computing the correlations.

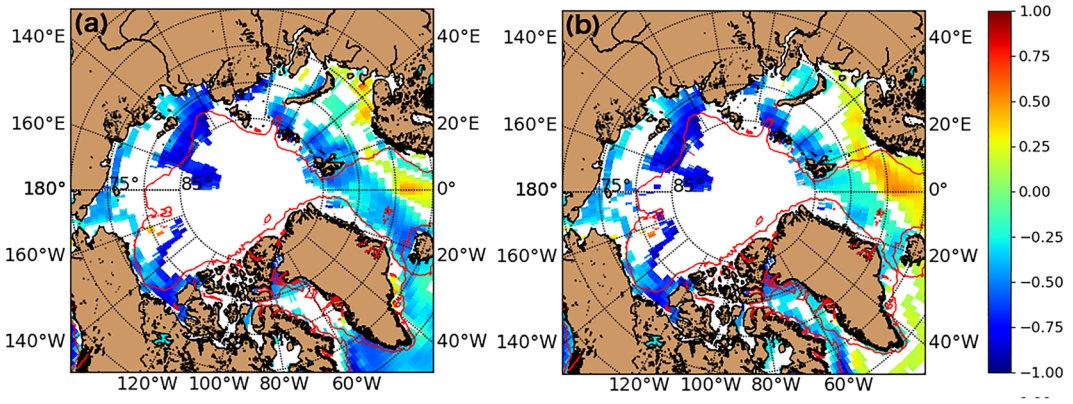

Figure 6. Regional distribution of temporal correlation coefficients during the period 1992–2015 between monthly ECCO-v4 SSS and sea surface height anomaly (SSHA) with the seasonal cycle included (a) and with the seasonal cycle removed (b). The red solid line represents the 500-m isobath contour. Only significant correlations (p value < 0.05) are shown. The monthly ECCO-v4 ice mask is applied to the model data before computing the correlations.

$R = -0.83$ averaged over the Arctic Ocean (>70°N) when the seasonal cycle is included and slightly better (−0.84) in the North American coasts, North Atlantic Ocean, Baffin Bay when the seasonal cycle is removed. The seasonal cycle is computed as the average of each month over the whole time series, this seasonal cycle is then subtracted from the monthly time series. This improvement might be related to the different responses of SSS and FWC to surface freshwater forcing or wind forcing on seasonal versus nonseasonal time scales. These are also regions of high sea ice formation and melt, leading to large surface salinification and freshening signals, respectively. It is beyond the scope of this study to identify exact causes for the difference between seasonal and nonseasonal correlation values. In regions shallower than 500 m (e.g., the Arctic shelves), SSS is a very good proxy for FWC, and to our knowledge the relationship between SSS and FWC in the upper Arctic Ocean has not been reported previously.

While SSHA-OBPA reflects steric height changes and is dominated by the halosteric contribution (Köhl, 2014; Morison et al., 2012; Pardaens et al., 2011), SSHA variations include mass contribution. However, if there are regions where mass contribution is small and thus SSS and SSHA correlation is strong, satellite SSH can be used directly as a proxy for FWC without relying on additional measurements from satellite OBPA that have much low resolution and shorter record.

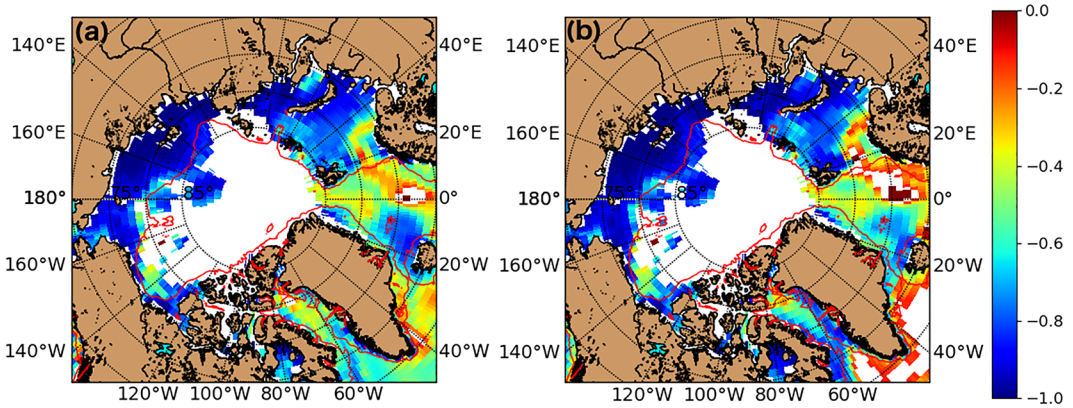

Figure 7. Regional distribution of temporal correlation coefficients during the period 1992–2015 between monthly ECCO-v4 SSS and SSHA-minus-OBPA with the seasonal cycle included (a) and with the seasonal cycle removed (b). The red solid line represents the 500-m isobath contour. Only significant correlations (p value < 0.05) are shown. The monthly ECCO-v4 ice mask is applied to the model data before computing the correlations.

Figures 6a and 6b show the spatial distribution of correlations between monthly SSS and SSHA with the averaged seasonal cycle included (Figure 6a) and excluded (Figure 6b). The two parameters are anticorrelated when averaged over the Arctic Ocean (for latitudes higher than 70°N), with correlation coefficients of −0.49 and −0.46 with and without including the seasonal cycle. When the seasonal cycle is included (Figure 6a), the maximum values of the anticorrelations (−0.8) are found in the Beaufort and Laptev seas; negative correlations are also found in some shelf areas (e.g., the Siberian Shelf), western subpolar North Atlantic, and a good part of the subpolar North Pacific (except near the Bering Strait). When the seasonal cycle is excluded (Figure 6b), the negative correlations in these regions either disappear or are reduced. In particular, the correlation between SSS and SSHA is weaker over the shelves. In the Norwegian Sea, Barents Sea, and North Atlantic Ocean, the correlation becomes positive (+0.3 to +0.5).

We hypothesize that the poor correlation between SSS and SSHA along the Arctic shelves is caused by the significant contribution of barotropic coastally trapped waves to SSHA variability in these region, especially for the nonseasonal anomalies. Fukumori et al. (2015) identified a pattern of coherent fluctuations in SSHA and OBPA across the Arctic Ocean and the Nordic Seas caused by coastally trapped barotropic waves excited by winds along the continental slopes of the Arctic Ocean, Nordic Seas, and the North Atlantic Ocean. These barotropic waves are unrelated to salinity or density variations, so their presence in SSHA would cause a reduction in correlation with SSS. Moreover, Peralta-Ferriz et al. (2014) used GRACE OBPA data to show that circulation in shallow regions of the Arctic Ocean, especially the Chukchi, East Siberian, and Laptev Seas, are dominated by barotropic signals.

Finally, we removed OBPA from SSHA and computed the correlation between SSS and SSHA-OBPA. There is a strong correlation around the Arctic Ocean shelves (Figure 7; within the 500-m isobath represented by the solid red line) and the correlation averaged over the Arctic Ocean (>70°N) is −0.73. The path of warm salty Atlantic water inflow in the Nordic and Barents Seas is highlighted by small (or negligible) correlation coefficients, reflecting the fact that steric sea level is more strongly influenced by temperature in these regions (Figure 7). In the Beaufort Gyre, the correlation between SSS and SSHA-OBPA ($R \sim -0.3$ to -0.4) is weaker than that along the Arctic shelves (discussed below). However, overall, the results demonstrate that SSS variability is coherent and strongly anticorrelated with those of SSHA-OBPA over much of the Arctic Ocean, especially in the shallow shelf regions.

To further illustrate the relationship between SSS and SSHA-OBPA, we compute the linear regression coefficient between SSS and SSHA-OBPA (Figure 8; in pss/cm). A large (small) regression coefficient indicates a strong (weak) relation between SSS and steric height changes. The regression coefficients are approximately −0.3 pss/cm or higher in magnitude in the shelf sea regions (within the 500-m isobath represented as a solid red line). In particular, regression coefficients reach −0.38 and −0.42 pss/cm near Bering Strait and in the Chukchi Sea, respectively. In deeper regions, such as the Beaufort Gyre and high-latitude North Atlantic, the regression coefficients have much smaller magnitudes, at −0.07 pss/cm and −0.05 pss/cm, respectively. The relationship between SSS and SSHA-OBPA is stronger over the Arctic shelves because freshwater inputs by river runoff and sea ice melt have large influence on the steric height signal, and the shelf regions are in general better mixed (less stratified) than the deep ocean. For example, the difference between salinity values averaged in the upper 10 m and over 10–200 m is 0.08 pss for regions shallower than 200 m (Figure 9, red curve). On the other hand, the same difference for regions deeper than 200 m is 2 pss (Figure 9, blue curve). This is consistent with the notion that SSS is a better proxy for column-integrated salinity in shallower regions such as the shelves than in the deeper oceans. In deeper regions, the relationship between SSS and SSHA-OBPA is weaker also because SSHA-OBPA signals are also affected by wind-driven Ekman transport, deeper halosteric changes that are not necessarily coherent with the SSS changes, and thermosteric effects. In the Beaufort Gyre, for example, steric sea level changes are dominated by the fluctuation of the halocline depth due to Ekman pumping (McPhee et al., 2009; Morison et al., 2012) which would not necessarily be reflected by a corresponding SSS signal.

We select two regions on the Arctic shelves to illustrate the temporal evolution of SSS and OBPA-SSHA: the Chukchi shelf (red square in Figure 8a) and the Siberian shelf (magenta square in Figure 8a). Here the sign of SSHA-OBPA is flipped (because it is anticorrelated to SSS), we compute the mean SSS and OBPA-SSHA in

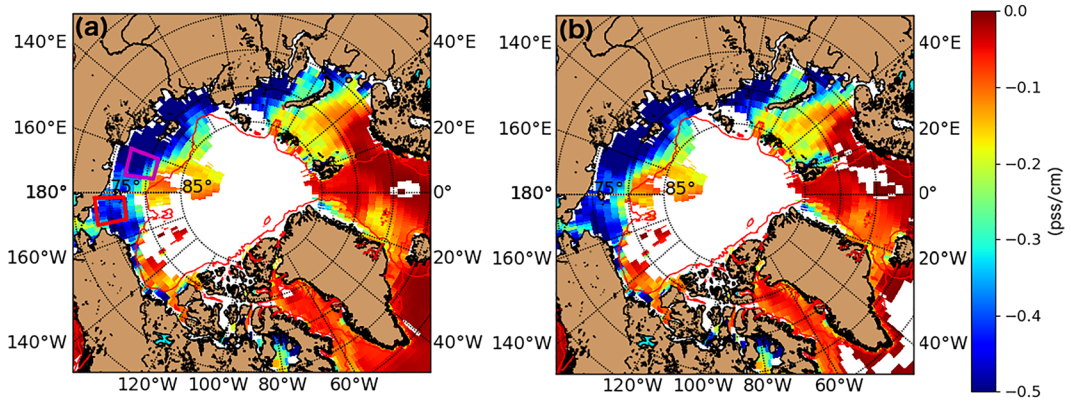

Figure 8. Regional distribution of the linear regression slope coefficients for the regression between monthly ECCO-v4 SSS and SSHA-minus-OBPA (a) with the seasonal cycle included and (b) with the seasonal cycle removed. The red solid line represents the 500-m isobath contour. The red and magenta squares (a) delimit respectively the Chukchi shelf and the Siberian shelf areas in which time series in Figure 9 are computed. Only significant correlations (p value < 0.05) are shown. The monthly ECCO-v4 ice mask is applied to the model data before computing the correlations.

each region, and the time series are normalized relative to the standard deviation (Figure 10). The two time series clearly show coherent variations, especially on interannual time scales. We find linear correlation coefficients of 0.52 and 0.97, and regression coefficients of −0.48 ± 0.1 and −0.51 ± 0.03 pss/cm, for the Chukchi and Siberian Sea regions, respectively.

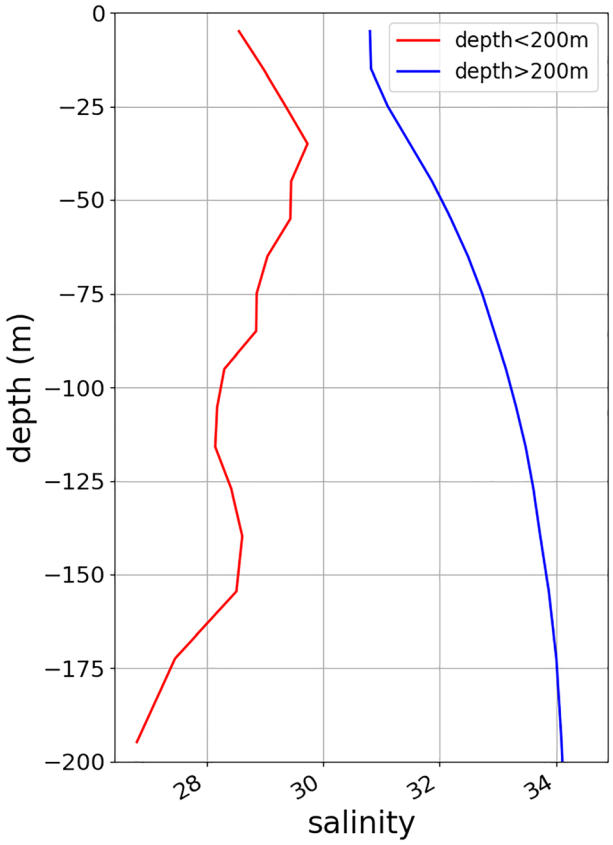

Figure 9. Average ECCO salinity profile over 1992–2015 at latitudes above 70°N, excluding the North Atlantic Ocean and the Barents Sea (e.g., excluding longitudes between 40°W and 60°E).

The results presented above have implications for the evaluation of the L band satellite SSS in the Arctic Ocean. Given the scarcity of in situ salinity data in the ice-free Arctic Ocean, SSHA-OBPA estimates can be used to assess the relative quality of satellite SSS retrievals. This is especially true in the shallow shelf sea regions, where the lack of in situ data is most acute and the relationship between SSS and SSHA-OBPA is strongest. The uncertainty of gridded satellite SSHA-OBPA is typically considered to be approximately 2 cm at high latitudes, and potentially larger on the shelf seas (Armitage et al., 2016; Chambers & Bonin, 2012). This uncertainty multiplied by the regression coefficient corresponds to a threshold of equivalent SSS change that the satellite SSHA-OBPA can help to determine, that is, too small a regression coefficient would correspond to too small an implied change of SSS for a given steric sea level signal. If the implied SSS change is smaller than the discrepancies among satellite SSS and the differences between satellite SSS with the limited in situ data in the Arctic Ocean as reported by Fournier et al. (2019), then satellite SSHA-OBPA data will not be helpful in evaluating the quality of satellite SSS. In this respect, a large regression coefficient is helpful because it corresponds to a large dynamic range of implied SSS change. The evaluation of satellite SSS using satellite SSHA-OBPA can only be performed at the resolutions resolved by satellite OBPA data (the lowest resolution of all three types of satellite data). In other words, satellite SSS and SSH need to be decimated to the spatial resolution of the OBPA data (~300 km). Therefore, satellite SSHA-OBPA will only be able to evaluate the averaged SSS for this spatial resolution, but not the SSS spatial variability smaller than this resolution (e.g., sharp SSS gradients associated with river plumes). In terms of the representativeness error of SSHA-OBPA in regions with sharp SSS gradients such as river plumes: Satellite SSHA has the spatial resolution to resolve the halosteric height associated with river plumes. Such halosteric height effect has no impact on OBPA because the latter reflects larger-scale barotropic wave signals.

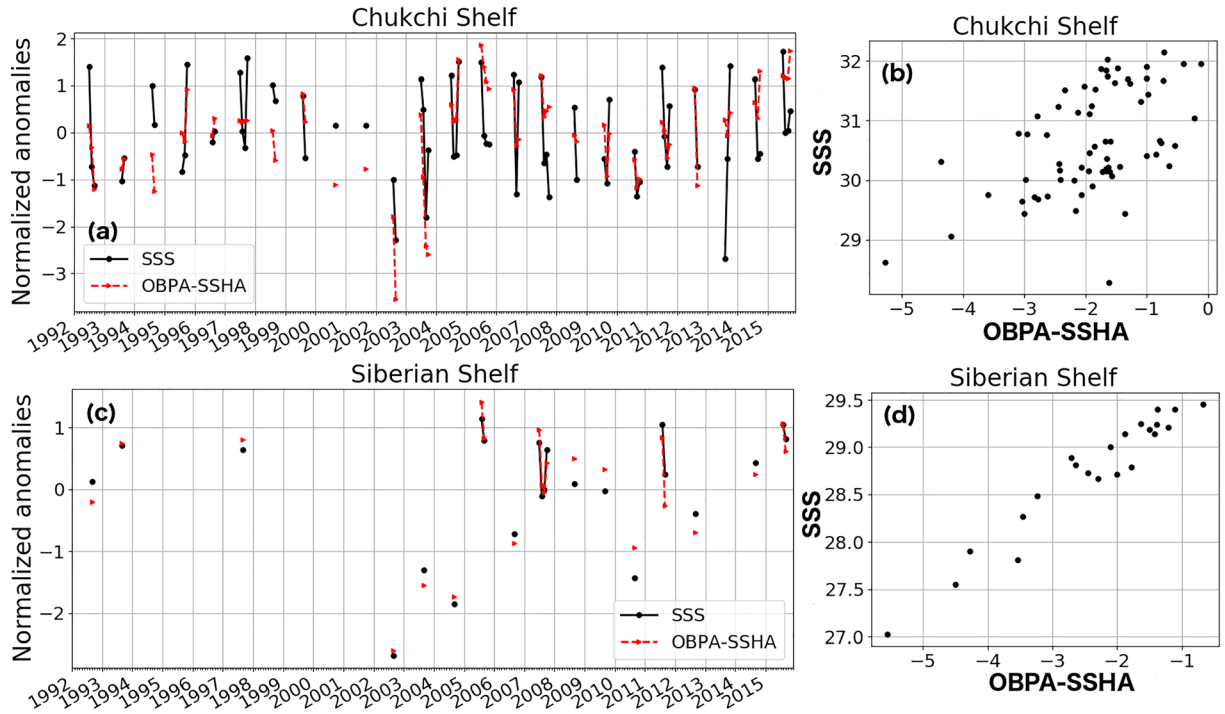

Figure 10. The 1992–2015 monthly time series of normalized ECCO-v4 sea surface salinity (SSS) (solid black line) and ocean bottom pressure anomaly (OBPA) minus sea surface height anomaly (SSHA) (dotted red line) on the Chukchi shelf (a) and Siberian shelf (c). Monthly SSS as a function of monthly OBPA-SSHA on the Chukchi shelf (b) and Siberian shelf (d). The Chukchi shelf and Siberian shelf areas are represented by a red and magenta squares, respectively in Figure 7. The monthly ECCO-v4 ice mask is applied to the model data.

4. Concluding Remarks

The potential of using SSS as a proxy for regional Arctic Ocean freshwater changes was investigated using the ECCO-v4 ocean-sea-ice state estimation product. The dynamically consistent state estimates reasonably reproduce the observed structure and variation of salinity compared to available in situ measurements, as well as the observed SSHA and OBPA variability in the Arctic Ocean. This provides us with the confidence to use the ECCO-v4 product to examine the relationship between SSS anomalies and depth-integrated FWC.

Analysis of the ECCO-v4 product shows that temporal variations of SSS are anticorrelated (−0.83) with the FWC when averaged over the Arctic Ocean (above 70°N). SSS variations over much of the Arctic Ocean are also found to be coherent with those of SSHA-OBPA, which reflect column-integrated steric height changes. Correlations between SSS and SSHA-OBPA are better than −0.8 over much of the Arctic Ocean except in the middle of the Beaufort Gyre and in the Barents Sea. In the Beaufort Gyre, the SSHA-OBPA signals are primarily caused by wind-driven Ekman pumping (Morison et al., 2012), thus having only a weaker anticorrelation with SSS. In the Barents Sea, positive correlations are found between SSS and SSHA-OBPA. This is believed to be caused by the covariability of salinity and temperature associated with the saltier and warmer Atlantic inflow, with the temperature effect dominating the SSHA-OBPA.

The results suggest that, overall, SSS is a good proxy for studying Arctic Ocean freshwater changes, especially in the shallower regions and to a lesser extent in the Beaufort Gyre. In the shallower regions (e.g., the Kara, Laptev, East Siberian, and Chukchi Seas), the linear regression coefficient between SSS and SSHA-OBPA is typically stronger than −0.3 pss/cm. ECCOv4 uses climatological seasonal river discharges. Intraseasonally and interannually varying river discharges, if introduced, would influence both SSSA, thereby inducing changes in SSHA-OBPA through the halosteric height effect. The change of halosteric height (reflected by SSHA-OBPA) per unit of SSSA change is expected to be independent of the time scale of river discharge. Therefore, we expect the relationship of SSSA and SSHA-OBPA to be applicable when intraseasonally and interannually varying river discharges are introduced. One source of uncertainty for the regression

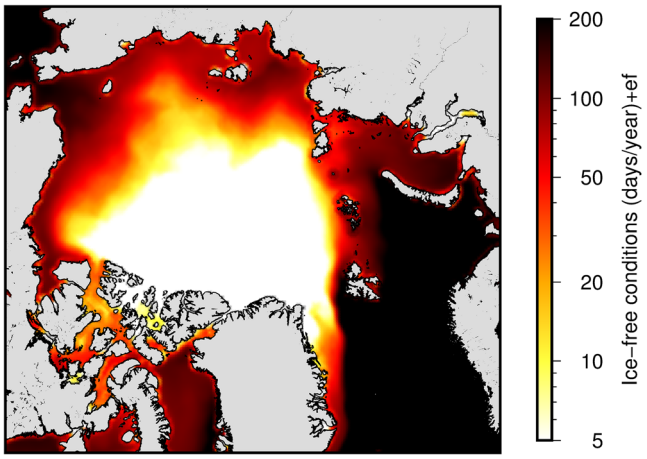

Figure 11. Average number of days per year that each pixel is free of ice.

coefficient between SSSA and SSHA-OBPA is the fidelity of ECCOv4 in representing the near-surface salinity stratification in regions affected by river plumes in the Arctic Ocean. More in situ measurements are needed to further evaluate the near-surface salinity stratification in these regions.

Our results also demonstrate the feasibility of using the relationship between SSS and SSHA-OBPA to evaluate satellite SSS retrievals in the Arctic Ocean using altimetry and gravimetry data. For example, the regression coefficients between SSSA and SSHA-OBPA represented by ECCOv4 or from the averages of the regression coefficients from an ensemble of ocean-sea ice state estimation products that have good fidelity can be used to represent the actual SSSA and SSHA-OBPA regression coefficients. Observed SSHA-OBPA can then be used to estimate the expected changes in SSSA by taking into account the errors of the observed SSHA and OBPA.

The ability to use SSS variation as a proxy for Arctic FWC changes also underscores the important need for technology innovation for improving salinity remote sensing in polar oceans, for example, beyond the single-frequency L band remote sensing technique. In order to assess the potential contribution of satellite SSS estimates to the overall Arctic Ocean FWC observing system, we use daily sea ice concentration from the NASA Bootstrap algorithm between 2000 and 2018 (Cavalieri et al., 1996). For each daily map, we set the ice presence to 1 for ice concentration greater than 0, and 0 otherwise. We then find the mean ice presence in days per year (Figure 11). In shelf sea regions, satellite SSS estimates could provide valuable spatially extensive estimates of FWC every 2–3 days for 1 to 3 months/year in the summer, representing an improvement on the current FWC observing system. We also note that this is under the scenario of the current 21st century sea ice conditions, and the coverage of satellite SSS estimates will improve as the ice cover further retreats under climate change.

Finally, realistic representation of the Arctic freshwater system in climate models remains to be a significant challenge (Jahn et al., 2012; Lique et al., 2016). Our results based on ECCO-v4, especially the relationship of SSS with halocline FWC and with steric height in the Arctic Ocean, can also be useful for evaluating climate models.

Acknowledgments

The research described in this paper was carried out at the Jet Propulsion Laboratory, California Institute of Technology, under a contract with NASA. Data Availability Statement Data for this paper are available at the following data centers we gratefully thank: the Jet Propulsion Laboratory for the ECCO-v4 model outputs (https://ecco.jpl.nasa.gov/products/latest); World Ocean Database (https://www.nodc.noaa.gov/cgi-bin/OC5/SELECT/dbsearch.pl) for CTD and XBT data; IFREMER (http://www.argodatamgt.org/) for Argo floats data; the International Council for the Exploration of the Sea (ICES) database (http://ices.dk/marine-data/data-portals/Pages/ocean.aspx) for in situ data; J. Toole and M.-L. Timmerman for Ice-Tethered profiler (ITP) measurements; WHOI (http://www.whoi.edu/beaufortgyre) for Beaufort Gyre mooring data; Wilken von Appen, Beth Curry, and Rebecca Woodgate for Fram Strait, Davis Strait, and Bering Strait mooring data.

References

Aagaard, K., Coachman, L. K., & Carmack, E. (1981). On the halocline of the Arctic Ocean. *Deep Sea research part a. Oceanographic Research Papers*, *28*(6), 529–545. https://doi.org/10.1016/0198-0149(81)90115-1

Andersen, O. B., & Knudsen, P. (2009). DNSC08 mean sea surface and mean dynamic topography models. *Journal of Geophysical Research*, *114*, C11001. https://doi.org/10.1029/2008JC005179

Armitage, T. W., Bacon, S., Ridout, A. L., Petty, A. A., Wolbach, S., & Tsamados, M. (2017). Arctic Ocean surface geostrophic circulation 2003–2014. *The Cryosphere*, *11*(4), 1767–1780. https://doi.org/10.5194/tc-11-1767-2017

Armitage, T. W. K., Bacon, S., Ridout, A. L., Thomas, S. F., Aksenov, Y., & Wingham, D. J. (2016). Arctic sea surface height variability and change from satellite radar altimetry and GRACE, 2003–2014. *Journal of Geophysical Research: Oceans*, *121*, 4303–4322. https://doi.org/10.1002/2015JC011579

Beszczynska-Möller, A., Fahrbach, E., Schauer, U., & Hansen, E. (2012). Variability in Atlantic water temperature and transport at the entrance to the Arctic Ocean, 1997–2010, ICES. *Journal of Marine Science*, *69*(5), 852–863. https://doi.org/10.1093/icesjms/fss056

BeszczynskA-Möller, A., Woodgate, R. A., Lee, C., Melling, H., & Karcher, M. (2011). A synthesis of exchanges through the main oceanic gateways to the Arctic Ocean. *Oceanography*, *24*(3), 82–99. https://doi.org/10.5670/oceanog.2011.59

Bintanja, R., & Andry, O. (2017). Towards a rain-dominated Arctic. *Nature Climate Change*, *7*(4), 263.

Bintanja, R., & Selten, F. M. (2014). Future increases in Arctic precipitation linked to local evaporation and sea-ice retreat. *Nature*, *509*(7501), 479–482. https://doi.org/10.1038/nature13259

Bulgakov, N. P. (1962). Determination of functional graphs of the time at which water reaches the freezing point and the depth of density mixing. *Problems of the North*, *4*, 141–148.

Carmack, E., McLaughlin, F., Yamamoto-Kawai, M., Itoh, M., Shimada, K., Krishfield, R., & Proshutinsky, A. (2008). Freshwater storage in the Northern Ocean and the special role of the Beaufort gyre. In *Arctic–subArctic ocean fluxes* (pp. 145–169). Dordrecht: Springer.

Carmack, E., Polyakov, I., Padman, L., Fer, I., Hunke, E., Hutchings, J., et al. (2015). Toward quantifying the increasing role of oceanic heat in sea-ice loss in the new Arctic. *Bulletin of the American Meteorological Society*, *96*(12), 2079–2105. https://doi.org/10.1175/BAMS-D-13-00177.1

Carmack, E., Winsor, P., & Williams, W. (2015). The contiguous panarctic riverine coastal domain: A unifying concept. *Progress in Oceanography*, *139*, 13–23. https://doi.org/10.1016/j.pocean.2015.07.014

Carmack, E. C., Yamamoto-Kawai, M., Haine, T. W. N., Bacon, S., Bluhm, B. A., Lique, C., et al. (2016). Freshwater and its role in the Arctic marine system: Sources, disposition, storage, export, and physical and biogeochemical consequences in the Arctic and global oceans. *Journal of Geophysical Research: Biogeosciences*, *121*, 675–717. https://doi.org/10.1002/2015JG003140

Cavalieri, D. J., Parkinson, C. L., Gloersen, P., & Zwally, H. J. (1996). Sea-ce concentrations from Nimbus-7 SMMR and DMSP SSM/I-SSMIS passive microwave data, version 1, edited, National Snow and Ice Data Center Distributed Data Archive Center, Boulder, Colorado USA

Chambers, D. P., & Bonin, J. A. (2012). Evaluation of Release-05 GRACE time-variable gravity coefficients over the ocean. *Ocean Science*, *8*(5), 859–868. https://doi.org/10.5194/os-8-859-2012

Chen, X.-Y., & Tung, K.-K. (2014). Varying planetary heat sink led to global-warming slowdown and acceleration. *Science*, 897–903. https://doi.org/10.1126/science.1254937

Curry, B., Lee, C. M., Petrie, B., Moritz, R. E., & Kwok, R. (2014). Multiyear volume, liquid freshwater, and sea-ice transports through Davis Strait, 2004 J. *Physical Oceanography*, *44*(4), 1244–1266. https://doi.org/10.1175/JPO-D-13-0177.1

Dee, D. P., Uppala, S. M., Simmons, A. J., Berrisford, P., Poli, P., Kobayashi, S., et al. (2011). The ERA-Interim reanalysis: Configuration and performance of the data assimilation system. *Quarterly Journal of the Royal Meteorological Society*, *137*(656), 553–597. https://doi.org/10.1002/qj.828

Entekhabi, D., Yueh, S., O'Neill, P., Kellogg, K. H., Allen, A., Bindlish, R., et al. (2014). *SMAP handbook soil moisture active passive: Mapping soil moisture and freeze/thaw from space, JPL CL14–2285*. Pasadena, CA: Jet Propulsion Laboratory.

Forget, G., Campin, J. M., Heimbach, P., Hill, C. N., Ponte, R. M., & Wunsch, C. (2015). ECCO version 4: An integrated framework for non-linear inverse modeling and global ocean state estimation. *Geoscientific Model Development*, *8*(10), 3071–3104. https://doi.org/10.5194/gmd-8-3071-2015

Fournier, S., Lee, T., Tang, W., Steele, M., & Omeldo, E. (2019). Evaluation and intercomparison of SMOS, Aquarius and SMAP sea surface salinity products in the Arctic Ocean. *Remote Sensing*, *11*(24), 3043. https://doi.org/10.3390/rs11243043

Fukumori, I., Wang, O., Fenty, I., Forget, G., Heimbach, P., & Ponte, R. M. (2017). ECCO version 4 realease 3, http://hdl.handle.net/1721.1/110380. https://1721.1/110380, Available at ftp://ecco.jpl.nasa.gov/Version4/Release3/doc/v4r3_summary.pdf

Fukumori, I., Wang, O., Llovel, W., Fenty, I., & Forget, G. (2015). A near-uniform fluctuation of ocean bottom pressure and sea level across the deep ocean basins of the Arctic Ocean and the Nordic seas. *Progress in Oceanography*, *134*, 152–172. https://doi.org/10.1016/j.pocean.2015.01.013

Garcia-Eidell, C., Comiso, J. C., Dinnat, E., & Brucker, L. (2017). Satellite observed salinity distributions at high latitudes in the northern hemisphere: A comparison of four products. *Journal of Geophysical Research: Oceans*, *122*, 7717–7736. https://doi.org/10.1002/2017JC013184

Giles, K. A., Laxon, S. W., Ridout, A. L., Wingham, D. J., & Bacon, S. (2012). Western Arctic Ocean freshwater storage increased by wind-driven spin-up of the Beaufort Gyre. *Nature Geoscience*. https://doi.org/10.1038/NGEO1379

Haine, T. W. N., Curry, B., Gerdes, R., Hansen, E., Karcher, M., Lee, C., et al. (2015). Arctic freshwater export: Status, mechanisms, and prospects. *Global and Planetary Change*, *125*, 13–35. https://doi.org/10.1016/j.gloplacha.2014.11.013

Häkkinen, S., & Proshutinsky, A. (2004). Freshwater content variability in the Arctic Ocean. *Journal of Geophysical Research*, *109*, C03051. https://doi.org/10.1029/2003JC001940

Heimbach, P., Hill, C., & Giering, R. (2005). An efficient exact adjoint of the parallel MIT general circulation model, generated via automatic differentiation. *Future Generation Computer Systems*, *21*, 1356–1371.

Jahn, A., Aksenov, Y., Cuevas, B. A., Steur, L., Häkkinen, S., Hansen, E., et al. (2012). Arctic Ocean freshwater: How robust are model simulations? *Journal of Geophysical Research*, *117*, C00D16. https://doi.org/10.1029/2012JC007907

Köhl, A. (2014). Detecting processes contributing to interannual halosteric and thermosteric sea level variability. *Journal of Climate*, *27*(6), 2417–2426. https://doi.org/10.1175/JCLI-D-13-00412.1

Köhl, A., & Serra, N. (2014). Causes of decadal changes of the freshwater content in the Arctic Ocean. *Journal of Climate*, *27*(9), 3461–3475. https://doi.org/10.1175/JCLI-D-13-00389.1

Kwok, R., & Rothrock, D. A. (2009). Decline in Arctic Sea-ice thickness from submarine and ICES at records: 1958–2008. *Geophysical Research Letters*, *36*, L15501. https://doi.org/10.1029/2009GL039035

Large, W., Yeager, S. (2004). Diurnal to decadal global forcing for ocean and sea-ice models: The data sets and flux climatologies (No. NCAR/TN-460+STR). University Corporation for Atmospheric Research. https://doi.org/10.5065/D6KK98Q6

Lee, T. (2016). Consistency of Aquarius sea surface salinity with Argo products on various spatial and temporal scales. *Geophysical Research Letters*, *43*, 3857–3864. https://doi.org/10.1002/2016GL068822

Li, W. K., McLaughlin, F. A., Lovejoy, C., & Carmack, E. C. (2009). Smallest algae thrive as the Arctic Ocean freshens. *Science*, *326*(5952), 539–539. https://doi.org/10.1126/science.1179798

Lique, C., Holland, M. M., Dibike, Y. B., Lawrence, D. M., & Screen, J. A. (2016). Modeling the Arctic freshwater system and its integration in the global system: Lessons learned and future challenges. *Journal of Geophysical Research: Biogeosciences*, *121*, 540–566. https://doi.org/10.1002/2015JG003120

Losch, M., Menemnelis, D., Campin, J. M., Heimbach, P., & Hill, C. (2010). On the formulation of sea-ice models. Part 1: Effects of different solver implementations and parameterizations. *Ocean Modelling*, *33*(1–2), 129–144. https://doi.org/10.1016/j.ocemod.2009.12.008

Manucharyan, G. E., & Spall, M. A. (2016). Wind-driven freshwater buildup and release in the Beaufort Gyre constrained by mesoscale eddies. *Geophysical Research Letters*, *43*, 273–282. https://doi.org/10.1002/2015GL065957

Marshall, J., Adcroft, A., Hill, C., Perelman, L., & Heisey, C. (1997). A finite-volume, incompressible Navier-Stokes model for studies of the ocean on parallel computers. *Journal of Geophysical Research*, *102*(C3), 5753–5766. https://doi.org/10.1029/96JC02775

Marshall, J., Hill, C., Perelman, L., & Adcroft, A. (1997). Hydrostatic, quasi-hydrostatic, and nonhydrostatic ocean modeling. *Journal of Geophysical Research*, *102*(C3), 5733–5752. https://doi.org/10.1029/96JC02776

McPhee, M. G., Proshutinsky, A., Morison, J. H., Steele, M., & Alkire, M. B. (2009). Rapid change in freshwater content of the Arctic Ocean. *Geophysical Research Letters*, *36*, L10602. https://doi.org/10.1029/2009GL037525

Meneghello, G., Marshall, J., Timmermans, M. L., & Scott, J. (2018). Observations of seasonal upwelling and downwelling in the Beaufort Sea mediated by sea-ice. *Journal of Physical Oceanography*, *48*(4), 795–805. https://doi.org/10.1175/JPO-D-17-0188.1

Morison, J., Kwok, R., Peralta-Ferriz, C., Alkire, M., Rigor, I., Andersen, R., & Steele, M. (2012). Changing arctic ocean freshwater pathways. *Nature*, *481*(7379), 66–70. https://doi.org/10.1038/nature10705

NOAA (2015). The Arctic report card, Tech. rep., NOAA Reports

Olmedo, E., Gabarró, C., González-Gambau, V., Martínez, J., Ballabrera-Poy, J., Turiel, A., et al. (2018). Seven years of SMOS sea surface salinity at high latitudes: Variability in Arctic and sub-Arctic regions. *Remote Sensing*, *10*(11), 1772.

Pardaens, A. K., Gregory, J. M., & Lowe, J. (2011). A model study of factors influencing projected changes in regional sea level over the twenty-first century. *Climate Dynamics*, *36*, 2015–2033. https://doi.org/10.1007/s00382-009-0738-x

Pavlis, N. K., Holmes, S. A., Kenyon, S. C., & Factor, J. K. (2012). The development and evaluation of the Earth gravitational model 2008 (EGM2008). *Journal of Geophysical Research*, *117*, B04406. https://doi.org/10.1029/2011JB008916

Peralta-Ferriz, C., Morison, J. H., Wallace, J. M., Bonin, J. A., & Zhang, J. (2014). Arctic Ocean circulation patterns revealed by GRACE. *Journal of Climate*, *27*(4), 1445–1468. https://doi.org/10.1175/JCLI-D-13-00013.1

Peterson, B. J., Holmes, R. M., McClelland, J. W., Vörösmarty, C. J., Lammers, R. B., Shiklomanov, A. I., et al. (2002). Increasing river discharge to the Arctic Ocean. *Science*, *298*(5601), 2171–2173.

Pivovarov, S., Schlitzer, R., & Novikhin, A. (2003). River runoff influence on the water mass formation in the Kara Sea. In R. Stein, et al. (Eds.), *Siberian River run-off in the Kara Sea: Characterisation, quantification, variability, and environmental significance*, *Proc. Mar. Sci.*, (Vol. 6, pp. 9–26). Amsterdam: Elsevier.

Polyakov, I. V., Beszczynska, A., Carmack, E. C., Dmitrenko, I. A., Fahrbach, E., Frolov, I. E., et al. (2005). One more step toward a warmer Arctic. *Geophysical Research Letters*, *32*, L17605. https://doi.org/10.1029/2005GL023740

Polyakov, I. V., Pnyushkov, A. V., Alkire, M. B., Ashik, I. M., Baumann, T. M., Carmack, E. C., et al. (2017). Greater role for Atlantic inflows on sea-ice loss in the Eurasian Basin of the Arctic Ocean. *Science*, *356*(6335), 285–291. https://doi.org/10.1126/science.aai8204

Proshutinsky, A., Bourke, R. H., & McLaughlin, F. A. (2002). The role of the Beaufort gyre in Arctic climate variability: Seasonal to decadal climate scales. *Geophysical Research Letters*, *29*(23), 2100. https://doi.org/10.1029/2002GL015847

Proshutinsky, A., Krishfield, R., Timmermans, M. L., Toole, J., Carmack, E., McLaughlin, F., et al. (2009). Beaufort gyre freshwater reservoir: State and variability from observations. *Journal of Geophysical Research*, *114*, C00A10. https://doi.org/10.1029/2008JC005104

Rabe, B., Karcher, M., Kauker, F., Schauer, U., Toole, J. M., Krishfield, R. A., et al. (2014). Arctic Ocean basin liquid freshwater storage trend 1992–2012. *Geophysical Research Letters*, *41*, 961–968. https://doi.org/10.1002/2013GL058121

Rabe, B., Karcher, M., Schauer, U., Toole, J. M., Krishfield, R. A., Pisarev, S., et al. (2011). An assessment of Arctic Ocean freshwater content changes from the 1990s to the 2006–2008 period. *Deep-Sea Research Part I*, *58*(2), 173–185. https://doi.org/10.1016/j.dsr.2010.12.002

Reul, N., Tenerelli, J., Chapron, B., Vandemark, D., Quilfen, Y., & Kerr, Y. (2012). SMOS satellite L-band radiometer: A new capability for ocean surface remote sensing in hurricanes. *Journal of Geophysical Research*, *117*, C02006. https://doi.org/10.1029/2011JC007474

Serreze, M. C., Barrett, A. P., Slater, A. G., Woodgate, R. A., Aagaard, K., Lammers, R. B., et al. (2006). The large-scale freshwater cycle of the Arctic. *Journal of Geophysical Research*, *111*, C11010. https://doi.org/10.1029/2005JC003424

Simmons, A., Uppala, S., Dee, D., & Kobayashi, S. (2006). ERA-interim: New ECMWF reanalysis products from 1989 onwards. *ECMWF newsletter* (Vol. 110, pp. 25–35). https://www.ecmwf.int/node/17713

Swift, C., & McIntosh, R. (1983). Considerations for microwave remote sensing of ocean-surface salinity. *IEEE Transactions on Geoscience Electronics*, *GE-21*(4), 480–491.

Talley, L. D. (2002). Salinity patterns in the ocean. In M.C. MacCracken, J. S. Perry (Eds.), *Encyclopedia of global change. Volume: The earth system: Physical and chemical dimensions of global environmental change* (pp. 629-640). Chichester: John Wiley & Sons, Ltd.

Tang, W., Fore, A., Yueh, S., Lee, T., Hayashi, A., Sanchez-Franks, A., et al. (2017). Validating SMAP SSS with in-situ measurements. *Remote Sensing of Environment*, *200*, 326–340. https://doi.org/10.1016/j.rse.2017.08.021

Tang, W., Yueh, S., Yang, D., Fore, A., Hayashi, A., Lee, T., et al. (2018). The potential and challenges of using soil moisture active passive (SMAP) sea surface salinity to monitor Arctic Ocean freshwater changes. *Remote Sensing*, *10*(6), 869. https://doi.org/10.3390/rs10060869

Toole, J., Krishfield, R., Timmermans, M.-L., & Proshutinsky, A. (2011). The ice-tethered profiler: Argo of the Arctic. *Oceanography*, *24*, 126–135.

Tsubouchi, T., Bacon, S., Naveira Garabato, A. C., Aksenov, Y., Laxon, S. W., Fahrbach, E., et al. (2012). The Arctic Ocean in summer: A quasi-synoptic inverse estimate of boundary fluxes and water mass transformation. *Journal of Geophysical Research*, *117*, C01024. https://doi.org/10.1029/2011JC007174

Vaughan, D. G., Comiso, J. C., Allison, I., Carrasco, J., Kaser, G., Kwok, R., et al. (2013). Observations: Cryosphere. In T. F. Stocker (eds.), *Climate Change 2013: The Physical Science Basis*, Contribution of Working Group I to the Fifth Assessment Report of the Intergovernmental Panel on Climate Change (Chap. 4, pp. 317–382). Cambridge, United Kingdom and New York, NY, USA: Cambridge University Press.

Woodgate, R. A., Weingartner, T. J., & Lindsay, R. (2012). Observed increases in Bering Strait oceanic fluxes from the Pacific to the Arctic from 2001 to 2011 and their impacts on the Arctic Ocean water column. *Geophysical Research Letters*, *39*, L24603. https://doi.org/10.1029/2012GL054092

Xie, J., Raj, R. P., Bertino, L., Samuelsen, A., & Wakamatsu, T. (2019). Evaluation of Arctic Ocean surface salinities from the Soil Moisture and Ocean Salinity (SMOS) mission against a regional reanalysis and in situ data. *Ocean Science*, *15*(5), 1191–1206. https://doi.org/10.5194/os-15-1191-2019